catalysts

MDPI

Article

The Effect of a Nitrogen-Based Ionic Liquid as a Coating over 1Pd9Ag/Al_2O_3 for the Selective Hydrogenation of 1,7-Octadiene *vs* 1-Octene

Revana Chanerika [1], Mzamo L. Shozi [1], Mirko Prato [2] and Holger B. Friedrich [1,*]

[1] School of Chemistry and Physics, University of KwaZulu-Natal, Durban 4000, South Africa
[2] Materials Characterization Facility, Istituto Italiano di Tecnologia, 16163 Genoa, Italy
* Correspondence: friedric@ukzn.ac.za

Abstract: The effect of tetrabutylammonium nitrate ($[N_{4444}][NO_3]$) was studied as a surface coating over 1Pd9Ag/Al_2O_3 and applied in the selective hydrogenation of 1,7-octadiene in a mixture with 1-octene. Weight loadings up to a surface of three monolayers (MLs) were investigated and a further comparison coating with 1-ethylimidazole ([EIM]) was carried out to assess anionic effects in the Solid Catalysts with an Ionic Liquid Layer (SCILLs). Catalysts were characterised by H_2-chemisorption, TGA-DSC, BET measurements, XPS, and HR-TEM. Catalytic studies showed that the uncoated and EIM-coated (10 wt%) catalysts gave nearly a 100% conversion of 1,7-octadiene and 1-octene with a selectivity mainly towards octane. Coating with $[N_{4444}][NO_3]$ at 1 ML significantly decreased the 1-octene conversion by almost 50%, as well as the selectivity to octane (38%) at close to a 100% diene conversion. However, no net gain in 1-octene in the output stream was noted. At 2 ML IL/EIM coverage, a further decline in 1-octene conversion and octane selectivity was found at a diene conversion of 75%. The selectivity to 1-octene steadily increased from over the bare catalyst (52%) to the EIM-coated (62%) catalyst and SCILL (75%). At 3 ML IL coverage, the diene conversion (35%) was significantly reduced due to mass transfer limitations of hydrogen through the thick IL layer. Characterisation of the used catalysts by TG and BET analyses confirmed a leaching of up to 14% of the ionic liquid in the SCILLs coated at 1 ML and 2 ML, with an increase in surface area noted. Furthermore, smaller particle sizes of the used catalysts showed that the metal–support interaction was re-established. These results confirm a mild ligand coordination between the nitrogen in the IL anion and Pd and Ag where the ionic liquid remained physisorbed over the surface of the catalyst. In addition, component miscibility tests revealed partial solubility of the diene in the ionic liquid, indicating the presence of solvent effects also.

Keywords: silver; palladium; selective hydrogenation; 1,7-octadiene; $[N_{4444}][NO_3]$; [EIM]; monolayer

check for updates

Citation: Chanerika, R.; Shozi, M.L.; Prato, M.; Friedrich, H.B. The Effect of a Nitrogen-Based Ionic Liquid as a Coating over 1Pd9Ag/Al_2O_3 for the Selective Hydrogenation of 1,7-Octadiene *vs* 1-Octene. *Catalysts* **2023**, *13*, 746. https://doi.org/10.3390/catal13040746

Academic Editors: Lalit Kumar Golani and Fan Zhang

Received: 31 January 2023
Revised: 24 March 2023
Accepted: 30 March 2023
Published: 13 April 2023

Copyright: © 2023 by the authors. Licensee MDPI, Basel, Switzerland. This article is an open access article distributed under the terms and conditions of the Creative Commons Attribution (CC BY) license (https://creativecommons.org/licenses/by/4.0/).

1. Introduction

In the petrochemical industry, dienes are commonly produced as by-products via thermal cracking of petroleum fractions. The feeds containing these are difficult to process further over different catalysts in downstream polymerisation units [1–4]. The presence of dienes among valuable olefins can lead to undesirable side reactions, affecting polymer quality, and can cause catalyst deactivation [1,5,6]. The development of green, efficient, and economical catalysts for diene hydrogenation has become an important priority in addressing industrial and environmental concerns [7,8]. The selective hydrogenation of dienes over metal nanoparticles (NPs)-supported catalysts is an effective reaction in removing dienes as catalyst poisons [4,9–11]. Currently, palladium- or gold-based catalysts are utilised for the partial hydrogenation of butadienes in order to reach a high selectivity to butenes [12–14] as these metals can provide a significant difference in binding energies of the diene and olefin molecules over the active sites [12,13,15,16]. In this instance, once an olefin molecule is formed in the first hydrogenation step, it is desorbed from the

catalyst surface or replaced by another diene molecule before finding a chance for further hydrogenation to form the undesired alkane [17].

The electronic characteristic of active metal sites of catalysts can be fine-tuned and thus can aid the performance of these catalysts [18,19]. The electron density on the active metal sites can be adjusted by introducing ligands, promoters, and secondary or tertiary metals [19]. Ionic liquids (ILs) offer an alternative choice to organic modifiers. They comprise a cation and anion pair and have tuneable properties that offer many structures with different physicochemical properties that provide a great degree of flexibility in controlling the catalytic performance [20]. The performance of these catalysts can be influenced by a filter or ligand effect, or both, which stem from the properties of the ionic liquid [21].

The filter effect results from the difference in reactant, intermediate, and product solubility, ultimately dictating their relative concentrations over the active sites. In contrast, the ligand effect deals with the electronic interactions between the ionic liquid and active metal centres, which consequently control the electron density on the metal and its interactions with different reactants and intermediates [22]. Kernchen et al. [23] showed that coating a catalyst with an ionic liquid layer enhances the selectivity for partially hydrogenated products in the hydrogenation of cyclooctadiene in an autoclave. The cyclooctene yield increased from approximately 40% to 70% upon coating a commercial Ni catalyst with 1-butyl-3-methylimidazolium octylsulfate.

Another study by Umpierre et al. [24] showed that a palladium catalyst coated with various imidazolium-based ionic liquids gave an approximately 100% selectivity towards butenes in the hydrogenation of 1,3-butadiene. Recently, Antonels et al. [25] showed that coating a silica-gel-supported ruthenium catalyst with a thin film of an imidazolium-based IL improved the selectivity towards the partial hydrogenation products of toluene. They proposed that the selectivity in these Ru-SCILLs (Solid Catalysts with an Ionic Liquid Layer) might be tuned by a complex interplay between ionic liquid, metal, and substrate/intermediate.

The influence of an ionic liquid layer on the interactions of hydrogen with a Pd-SCILL was reported by Arras et al. [26]. Their results revealed the coordination between the active Pd and the anion of the ionic liquid (dicyanamide) and showed that the interaction decreased hydrogen uptakes and integral heats of adsorption, consequently controlling the adsorption of hydrogen onto the metal sites. In addition, Bauer et al. [27] illustrated that ionic liquid molecules interact with the active sites through their anions and form a mixed/dense matrix with the adsorbed reactants. The dense matrix offered a ligand-like effect over the active sites. Thus, coating supported metal catalysts with ionic liquids to implement the SCILL effect offers a means of controlling the electronic nature of the active sites and their selectivity to the desired products [12,28].

In our previous study focussing on the competitive hydrogenation of 1-octyne in 1-octene catalysed by Pd-SCILLs, it was noted that the activity of Pd was high and no net 1-octene gain in the product was achieved at full octyne conversion below an IL (1-butyl-3-methylimidazolium dicyanamide) loading of 45 wt% [29]. Hence, silver was incorporated to disperse neighbouring Pd atoms in an attempt to improve the overall selectivity to 1-octene and lower the surface area of metallic Pd. This gave a selective 1-octene catalyst, which was further investigated in this study. Ammonium-based ionic liquids are generally more stable than imidazolium-based ionic liquids and can be used at a higher temperature than imidazolium ILs. SCILL systems for selectively removing dienes as poisons from terminal olefin feedstocks have commonly only been reported for C_4 feeds with precious group metals such as Pd and Ag. To the best of our knowledge, no literature exists on the terminal activation of 1,7-octadiene (2 wt%) in the presence of 1-octene (10 wt%) using $PdAg/Al_2O_3$ coated with tetrabutylammonium nitrate.

It is expected that tetrabutylammonium nitrate ($[N_{4444}][NO_3]$) (containing hard electron-donating elements) offers the advantage of mild coordination to the active sites compared to soft-electron-donating elements (ligand effect) [30,31]. Hence, reactant binding energies

can be modified by the ionic liquid, where the 1,7-octadiene is expected to be more strongly adsorbed on the catalyst sites than the 1-octene due to it being more electron-deficient [12,27]. In this way, the selectivity to 1-octene is expected to improve.

2. Results and Discussion

Hydrogen uptakes and dispersion values of the IL-coated bimetallic catalysts are shown in Table 1. There were marked differences in dispersion between the bare and SCILL systems, showing the possibility of greater IL–metal interactions that weaken metal–support interactions and cause agglomeration. Thus, a large decrease in dispersion was observed from the bare (7.40%) to the coated catalysts (1.31% at 1 monolayer (ML) and 1.00% at 2 ML). This result was further confirmed with TEM techniques shown later in this report. Hydrogen uptakes (Table 1) were significantly reduced at 1 ML IL coverage compared to the bare catalyst (0.14 cm^3/g *vs* 0.79 cm^3/g) with a further decrease at 2 ML (0.11 cm^3/g). These H_2 uptake values of the 1Pd9Ag-14%[N_{4444}][NO_3] and 1Pd9Ag-24%[N_{4444}][NO_3] catalyst support the expectation of good catalytic performance in the selective hydrogenation of 1,7-octadiene up to a 2 ML coverage of IL.

Table 1. Physicochemical properties of the fresh uncoated and SCILLs up to 2 ML.

IL/Organic Modifier	H_2 Uptake (cm^3/g)	Dispersion (%)
1Pd9Ag/Al_2O_3	0.79	7.40
1Pd9Ag-14%[N_{4444}][NO_3]	0.14	1.31
1Pd9Ag-24%[N_{4444}][NO_3]	0.11	1.00

2.1. Competitive Hydrogenation of 1,7-Octadiene vs 1-Octene

Figure 1 shows the conversions of 1,7-octadiene and 1-octene (with standard deviations of <2%) over the bare, 1-ethylimidazole (EIM), and IL-coated catalysts at different loadings. Conversions of 1,7-octadiene over the bare catalyst reached 98%, with only a small decrease to 92% over the catalyst coated with the IL at a surface coverage of 1 ML. However, the conversion of 1-octene was almost halved (from 94% shown over the bare catalyst to 49% over the IL-modified catalyst) at 1 ML. These results show that reactant access to the active sites was hindered by the presence of the ionic liquid, which can potentially form multiple layers on the surface of the catalyst (exceeding 1 ML coverage) and thus induce mass transfer and diffusional limitations to the incoming reactants and hydrogen (Table 1). The results in Figure 1 support this, as doubling and tripling the IL coverage decreased the 1,7-octadiene and 1-octene adsorption over the surface, consequently suppressing their conversions. At 3 ML, where diene conversions were significantly lowered (35%) compared to the other tested catalysts, accessibility to the active sites was significantly diminished likely for two reasons: (i) the reactants are diffusion-limited and gas solubilities and mobilities are lower through the thick IL film on the surface of the catalyst, and (ii) the steric bulk of the ionic liquid allows minimal diffused reactant to adsorb over the active sites. For this reason, for any 1,7-octadiene molecule adsorbed on the surface, the ionic liquid expels the resultant hydrogenated product, 1-octene, and allows another incoming 1,7-octadiene molecule to adsorb rather than allowing the readsorption of 1-octene to form octane. These findings were confirmed by solubility tests that showed the immiscibility of 1-octene and hexane, but partial solubility of the diene, within the IL (Figure S1, Supplementary Materials). As such, both ligand and solvent effects controlled the selectivity. As substrate conversions were significantly lowered at multilayer coverage (beyond 2 ML), isoconversion results are provided for 1 ML and 2 ML coverages, in keeping with suitable 1,7-octadiene conversions (close to 100%) [32].

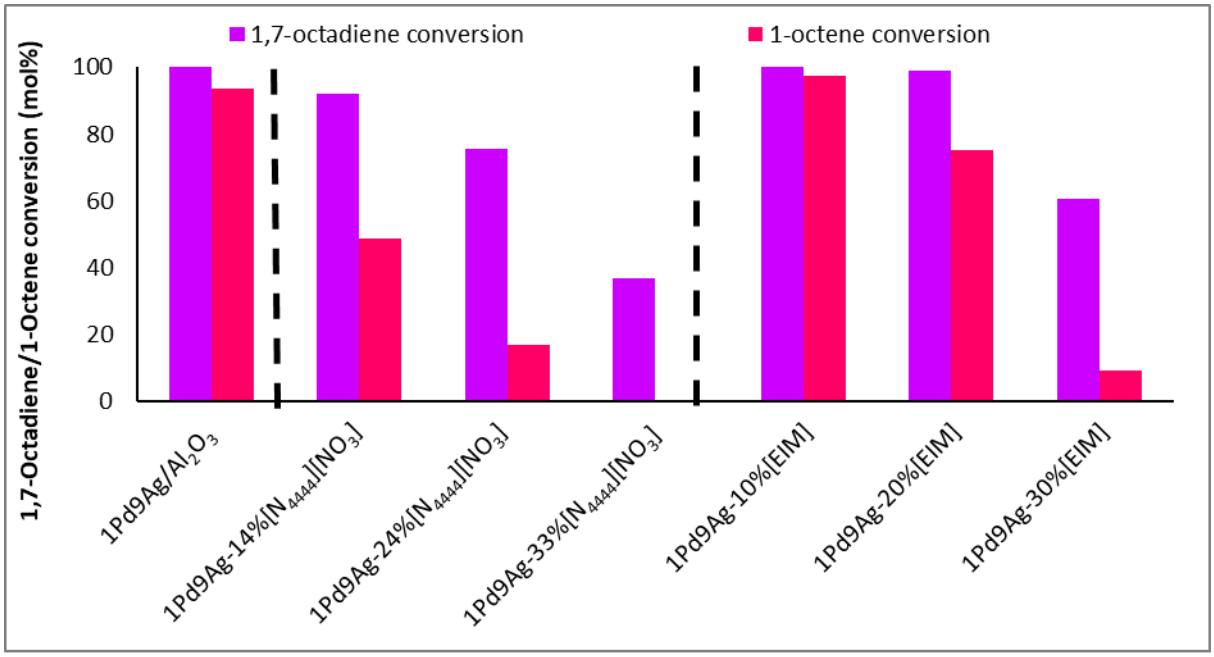


Figure 1. Conversion of 1,7-octadiene and 1-octene over 1Pd9Ag-14%[N_{4444}][NO_3]. **Reaction conditions:** Temperature: 100 °C, Pressure: 30 bar, Diene:H_2 ratio: 1:3.5, LHSV: 9 h^{-1}, Feed: 2 wt% 1,7 octadiene, 10 wt% octene in hexane.

Comparing the SCILLs with a catalyst coated with the organic modifier, 1-ethylimidazole, at 1 ML coverage showed that under the same reaction conditions, the conversions of 1,7-octadiene and 1-octene were distinctly different. Whilst near full 1,7-octadiene conversions were achieved over both the organically modified catalysts (up to 2 ML coverage) and the SCILL (for 1 ML coverage), 1-octene conversion was inhibited to a greater extent over the SCILL. A minimal effect of the organic modifier was noted, where substrate conversions resembled those of the bare catalyst. This poor effect of EIM may be because the ligand effect is very weak and the presence of an anion is needed to suppress 1-octene conversions substantially. Effects of surface modification with EIM became more visible at double and triple theoretical monolayer coverage with a steady decline in the conversion of 1-octene, with possible EIM arrangements shown in Figure 2. At a 30% loading (3 ML) of the organic modifier, 1,7-octadiene conversions significantly declined below acceptable values, which are ideally 100% [32], due to greater steric hindrance caused at the metal surface. Solubility tests showed the immiscibility of EIM with 1,7-octadiene, 1-octene, and the hexane solvent (Figure S1, Supplementary Materials). These findings showed ligand and solvent effects where both contributed to the decline in 1-octene conversion over the catalysts coated with 2 ML and 3 ML EIM.

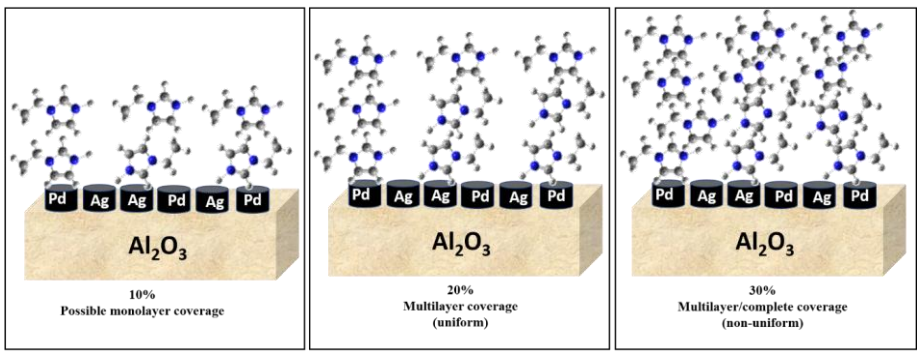


Figure 2. Different possible coverages associated with different EIM loadings.

As seen in Figure 3, there was a relatively low content of the targeted 1-octene in the output stream over both the uncoated and EIM systems. There was no gain in 1-octene (the amount detected solely from the hydrogenation of 1,7-octadiene) in the effluent stream over both the uncoated and SCILL systems. Increased octane formation was expected, because initially, when no IL coating is present, the reducible groups of the reactants are essentially the same and compete for the same reaction sites. With no diffusion barriers on the surface of the catalyst, i.e., from ionic liquids or carbonaceous deposits, active metal sites are available to adsorb the dissociated hydrogen to an extent where energetic hydrogen species can form (sub-surface and bulk hydrogen) [33]. This species is usually responsible for the formation of octane. Coating the ionic liquid to 1 ML gave a SCILL effect where the selectivity to octane was significantly reduced (from 88% over the bare catalyst to 50% over the SCILL) and the total content of 1-octene detected in the output stream was significantly higher (44%) than found over the bare catalyst (5%). The formation of octene isomers was also impeded upon coating, suggesting that the ionic liquid efficiently covered acidic sites that would otherwise initiate the isomerisation of 1-octene. This effect was also seen in previous work with Ag-SCILLs [34].

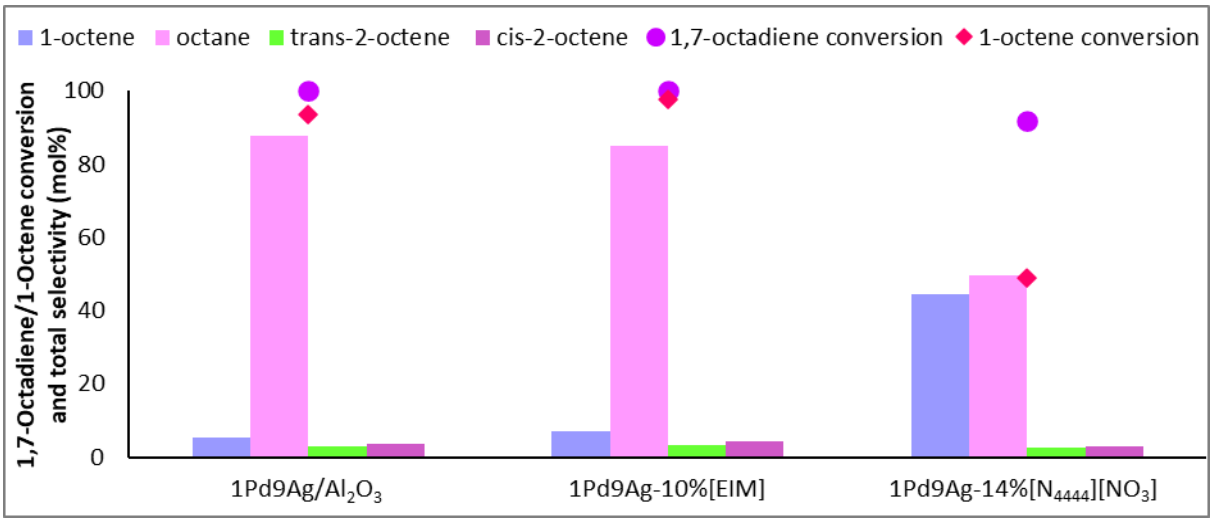


Figure 3. Selectivity profile of 1-octene, internal octenes, and octane over 1Pd9Ag-14%[N_{4444}][NO_3]. **Reaction conditions:** Temperature: 100 °C, Pressure: 30 bar, Diene:H_2 ratio: 1:3.5, LHSV: 9 h^{-1}, Feed: 2 wt% 1,7 octadiene, 10 wt% octene in hexane.

Another study on the competitive hydrogenation of 1,7-octadiene *vs* 1-octene using a 29 wt% Ni/Al_2O_3 catalyst coated with various sulphur-based ionic liquids ([MMIM][OcOSO3], [MMIM][MeOSO3], [MMIM][NTf]), at 10% and 25% weight loadings, showed high selectivities to octane (~70–85%) [35], whereas in our present study employing ammonium-based SCILLs, the content of octane was significantly reduced (50%) at close to 100% diene conversion. The authors suggested the possibility of site-specific interactions of the ionic liquid with the active metal. Complimentary to this argument, it was shown by Bauer et al. [27] that the IL, [EMIM][NTf_2], preferentially blocked low coordinated sites on nanoparticles [36]. Alkenes are generally regarded to react faster on flat sites as a result of steric hindrance to its adsorption on terraces [37]. This means that at 1 ML coverage, there were sites still favourable for the adsorption of both substrates, allowing for interactions of the diene and 1-octene with exposed flat sites. The selectivity profile of the catalyst coated with the organic modifier resembled that of the uncoated catalyst, showing that there were partial or insignificant mass transfer effects and ligand effects did not effectively impede the rate of readsorption of 1-octene.

At an isoconversion of 1,7-octadiene of 75 ± 2%, comparing the bare and 2 ML-coated catalysts (Figure 4), the conversion of 1-octene as well as the selectivity of octane were halved. Although there would be complete coverage of the active sites by 2 monolayers (a loading of 22 wt%) of the ionic liquid, it was insufficient to bring about a gain in 1-octene.

This highlights the possibility of weak coordination occurring between the anion (hard-nitrogen-containing donor) of the IL and the metal sites, allowing for incoming liquid and gaseous reactants to adsorb onto exposed active sites within the IL–metal interface. Due to the bulkiness of the ionic liquid and although the "on-top" configuration is energetically favoured for less basic anions [21,38,39], ions arrange to reduce repulsion where the anions and cations can alternate in a "side to side" fashion to avoid the repulsion of anions next to each other [40]. In this way, the available sites between the layers of the ionic liquid can accumulate gaseous and liquid reactants. Hence, at 2 ML coverage, the conversion of 1,7-octadiene was still relatively high and, compared with results over the organically (EIM) modified catalyst (which showed only a slight increase in 1-octene selectivity compared to the bare catalyst), there was still a strong effect shown by the SCILL, which showed a reduction in octane selectivity as well as halving the conversion of 1-octene.

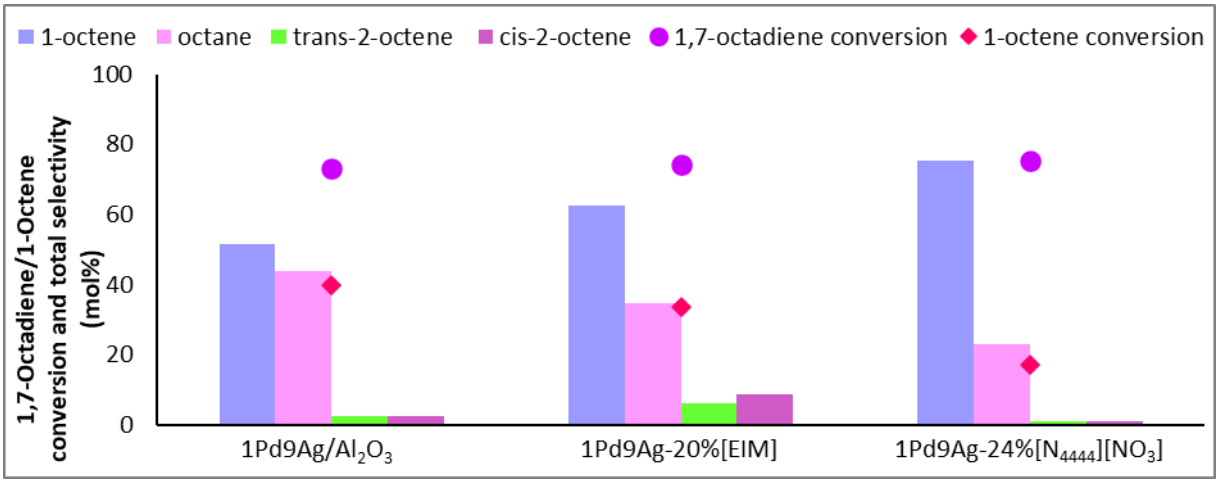


Figure 4. Selectivity profile of 1-octene, internal octenes, and octane over 1Pd9Ag-22%[N_{4444}][NO_3]. **Reaction conditions:** Temperature: 100 °C, Pressure: 30 bar, Diene:H_2 ratio: 1:3.5, LHSV: 9 h^{-1}, Feed: 2 wt% 1,7 octadiene, 10 wt% octene in hexane.

With an IL loading of 33 wt%, corresponding to a theoretical IL coverage of 3 ML (Figure 5), constant conversions of 1,7-octadiene (~35%) were noted over an 8 h time-on-stream, with a low selectivity to octane. With multiple layers of IL on the surface of the catalyst, the accessibility of reactants and hydrogen to the active sites was severely reduced, likely due to mass transfer limitations induced by the ionic liquid. In this case, the arrangement of the ions may be lost in the bulk with a random orientation with access to the metal sites being hindered by the thick film of ions packed over the active sites. For this reason, any 1,7-octadiene molecule that was adsorbed onto the active site was immediately hydrogenated to give 1-octene and expelled by the ionic liquid before having a chance to readsorb onto the surface and form octane. The diene molecule could then be replaced by another until it was completely consumed [12]. At this coverage, the conversion of 1-octene was almost zero; however (Figure 5), the low conversion of the diene makes utilisation of this IL, at a loading of 33 wt%, unsuitable, as the overall aim was to reduce the diene concentration to acceptable limits, preferably to zero [32], whilst maintaining high selectivity to 1-octene. The constant selectivity throughout the time-on-stream may be due to the IL layer regulating the relative concentrations of the diene, octene, and intermediates, where their removal from the surface due to the IL prevents coke build up (filter effect) [6,12].

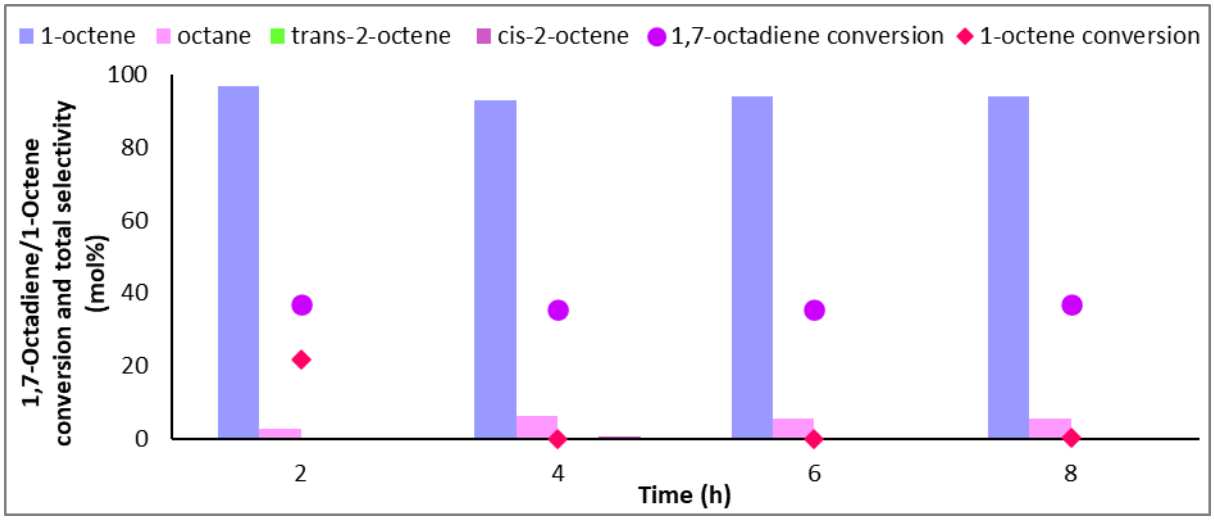


Figure 5. Conversion of 1,7-octadiene and 1-octene and selectivity to 1-octene, octane, and internal octenes over 1Pd9Ag-33%[N_{4444}][NO_3]. **Reaction conditions:** Temperature: 100 °C, Pressure: 30 bar, Diene:H_2 ratio: 1:3.5, LHSV: 9 h^{-1}, Feed: 2 wt% 1,7 octadiene, 10 wt% octene in hexane.

Turn-over frequencies (TOFs) based on 1,7-octadiene were calculated to assess the intrinsic performance of the catalysts (unmodified, organically modified, and SCILL) at 1 ML coverage. The trends in Table 2 provide supplemental evidence on the performance of the catalysts where the unmodified system gave the highest activity, whilst the SCILL was least active among the series of tested catalysts (0.19×10^{-3} s^{-1}). The space–time yield (STY) of 1-octene was observed to increase in the same order as the 1-octene selectivity (Figure 3). The SCILL gave the highest space–time yield, threefold and twofold higher than over the bare and organically modified catalysts, respectively. A small improvement in STY was observed over the EIM-coated catalyst compared to the unmodified catalyst. The increase in 1-octene STY over the SCILL showed that the ionic liquid indeed allowed access to necessary sites for diene hydrogenation, whilst limiting side reactions by blocking sites responsible for those.

Table 2. Turn-over frequencies (TOFs) and 1-octene space–time yield (STY) of the catalysts at 1 ML coverage.

Catalyst	TOF (s^{-1})	1-Octene STY ($g \cdot kg^{-1} \cdot h^{-1}$)
1Pd9Ag/Al_2O_3	1.79×10^{-3}	21.36
1Pd9Ag-10%[EIM]	0.50×10^{-3}	26.85
1Pd9Ag-14%[N_{4444}][NO_3]	0.19×10^{-3}	56.65

2.2. Non-Competitive Hydrogenation Studies

The contribution of the sorption factor to the rate and selectivity of diene hydrogenation is a result of the difference in behaviour of the alkadienes and alkenes in competitive and non-competitive hydrogenation reactions. In the case of alkadiene and alkene mixtures, alkadienes react faster than alkenes [41–43], whereas in non-competitive hydrogenation, alkenes react faster [44]. In general, the adsorption of a molecule on the surface of a metal catalyst is governed by its level of unsaturation. If a species is too strongly adsorbed on the surface of a catalyst, it may not react.

Figure 6 shows results of the non-competitive hydrogenation of 1,7-octadiene and 1-octene comparing the behaviour of the prepared SCILLs and organically modified catalysts *vs* the uncoated systems. The most active coated systems were chosen, which ideally represented coverage at 1 ML. From Figure 6a, it is evident that 1,7-octadiene was readily adsorbed on the surface when no IL was present and there were no mass transfer limitations

to sterically hinder access of the diene to the metal sites. Previous XPS studies showed an alloy formation between Pd and Ag, implying a larger negative charge on Pd due to electron donation from Ag. Hence, as soon as the octadiene is hydrogenated to octene and the *n*-octane, another diene molecule occupies the surface until complete consumption of the diene is achieved (100%). Coating with $[N_{4444}][NO_3]$ at a coverage of a single monolayer showed that although active Pd and Ag sites were sterically hindered by the IL, the arrangement of the IL allowed space between the adsorbing ions to accommodate and adsorb 1,7-octadiene to give full conversion. At this conversion, the role of the ionic liquid was dominantly seen by its ability to reduce the content of octane formed over the bare catalyst (82%) to the SCILL (56%). At the same instance, the total content of 1-octene detected by employing the SCILL increased two-fold compared to the uncoated catalyst. This shows that the active sites were hindered to a degree, reducing side reactions that would otherwise take place in the absence of the IL coating (Figure 6a).

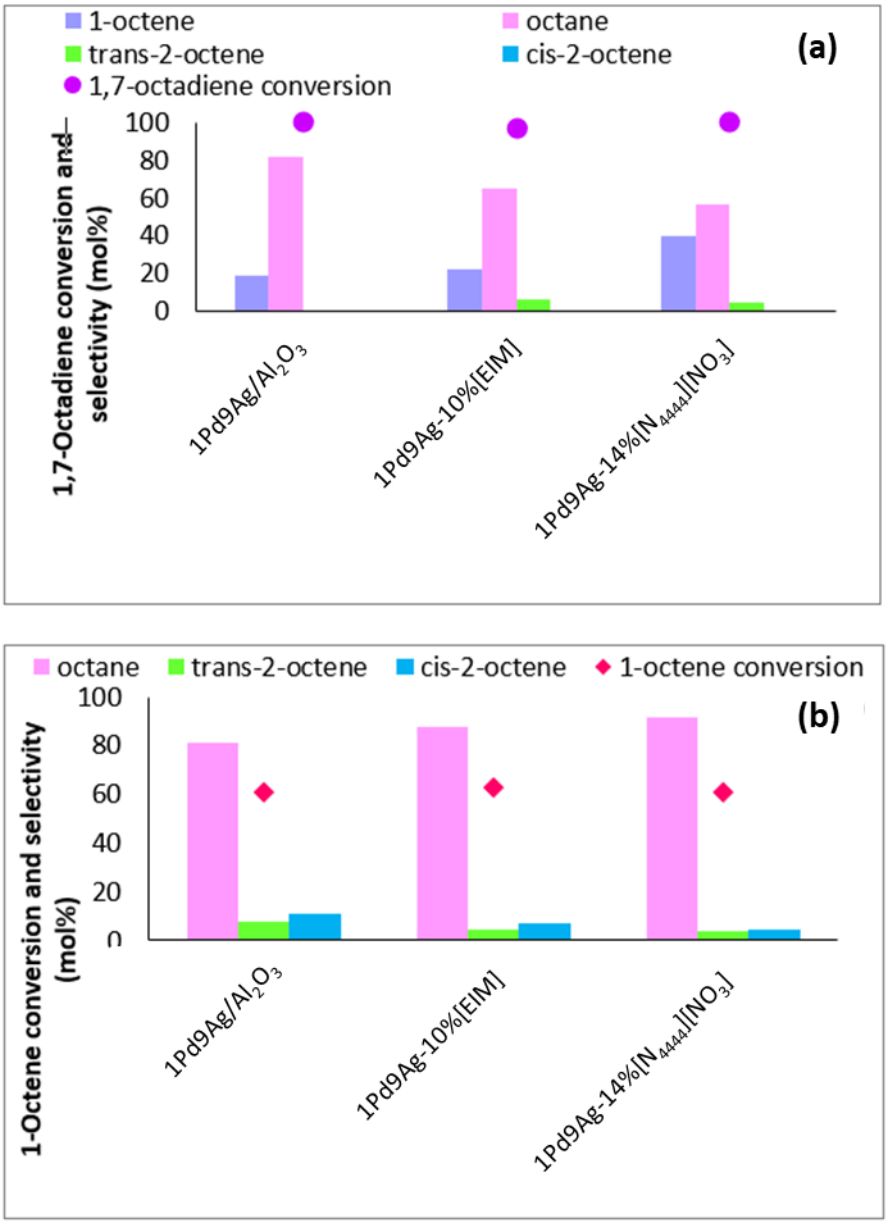


Figure 6. Non-competitive hydrogenation studies using (**a**) 1,7-octadiene and (**b**) 1-octene in hexane over $1Pd9Ag/Al_2O_3$ and 1Pd9Ag-14%$[N_{4444}][NO_3]$. **Reaction conditions:** Pressure: 30 bar, Diene:H_2 ratio: 1:3.5, Temperature: 100 °C. The standard deviation for values at 6 h is ± 0.2 mol%.

In the non-competitive hydrogenation of 1-octene in the hexane experiment (Figure 6b), conversions were significantly lower than those of the diene. Thus, 1-octene's adsorption on the surface occurred at significantly lower levels than 1,7-octadiene on all catalysts. To enable a product selectivity comparison between the uncoated, organically modified, and SCILL systems, 1-octene results were compared at 60% isoconversion. Coating with the ionic liquid showed a reduction in the internal octene isomers detected compared to the product over the uncoated catalyst as a result of surface acid site coverage by the IL. The increased selectivity to octane showed that, like the non-competitive diene reaction (Figure 6a), 1-octene was still adsorbed on the surface between the ions of the IL. In this case, the increased content of octane noted from the bare catalyst to the SCILL could imply that the IL avails sites specific to the adsorption of 1-octene (mainly flat surfaces) [45].

The use of the organic modifier (EIM) as a surface coating in each non-competitive hydrogenation reaction showed marked differences in the product selectivity and substrate conversions (Figure 6a,b). Whilst full 1,7-octadiene conversion was achieved, suppressed 1-octene conversion was noted as a result of its weak sticking coefficient compared to 1,7-octadiene, as well as the presence of EIM causing steric hindrance for any adsorbing 1-octene on the catalyst surface. The content of total 1-octene produced from the hydrogenation of 1,7-octadiene was nearly comparable to the amount produced over the bare catalyst, whilst octane formation was significantly supressed. This shows that the organic modifier on the surface at 1 ML (10%) indeed reduced the over-hydrogenation rate.

1-Octene showed to be readily adsorbed on the catalyst surface in the absence of a competing component (octadiene) as at substantial 1-octene conversions, 1-octene was readsorbed, producing octane from its hydrogenation (Figure 6b) even in the presence of EIM and the IL.

2.3. IL Leaching Tests

Mass loss percentages from the TGA analyses of the fresh and used bare and SCILL systems are reported in Table 3. The TG profiles showed mass losses attributed to moisture on the surface and within the pores (second-mass-loss DTG peak) of the fresh and used uncoated catalysts (Figure S2 (Supplementary Materials)). These weight losses were significantly lower in the SCILL systems due to pore blocking by the ionic liquid (Table 3). The mass loss percentages of the fresh SCILLs showed complete decomposition of the ionic liquids (15%, 23%, and 34%), corresponding to the expected loss of their theoretical loadings for 1 ML, 2 ML, and 3 ML of the ionic liquids, respectively. In the used SCILLs, however, ionic liquid leaching was significant at 2 ML and 3 ML with weight losses in the IL decomposition region of 13% and 20%, respectively (compared to weight losses of 23% and 34% in their fresh counterparts, respectively), whilst leaching at 1 ML was low (12% *vs* 15% in the fresh catalyst). This shows that as the content of IL was raised, the IL layers above the monolayer became bulk-like in nature, damping its interaction with the surface.

Table 3. Thermal analysis data for the fresh and used SCILLs.

Catalyst	Moisture (%)	IL wt Loss (%)	Total Weight Loss (%)
1Pd9Ag-14%[N_{4444}][NO_3] (fresh)	5	15	20
1Pd9Ag-14%[N_{4444}][NO_3] (used)	3	12	15
1Pd9Ag-24%[N_{4444}][NO_3] (fresh)	5	23	28
1Pd9Ag-24%[N_{4444}][NO_3] (used)	4	13	17
1Pd9Ag-33%[N_{4444}][NO_3] (fresh)	2	34	36
1Pd9Ag-33%[N_{4444}][NO_3] (used)	4	20	24

The ionic liquid used in this work showed a potential coordination arising only from the anion. It is unlikely that the cation will have strong interactions with the metal sites due to repulsion between them. Hence, as the ionic liquid layer grows, its interaction with the surface becomes weaker, and a spatial distribution of the IL over the surface results as the IL leaches. In the used SCILLs, a secondary effect is implied whereby increased support

interactions would usually initiate the decomposition of the ionic liquid when its coverage becomes more non-uniform and leads to more support sites being exposed [46–49].

BET surface measurements of the most active catalysts (up to 2 ML coverage) were carried out to assess the effects of coating the bare catalyst with different loadings of $[N_{4444}][NO_3]$. Significant changes within the catalyst pores were noted and the data are shown in Table 4 and Figure S3 in the Supplementary Materials. For the used uncoated catalyst, decreases in surface area, pore volume, and pore size were attributed to the deposition of carbonaceous material within the pores of the catalyst, causing blockages at the pore entrances. The postulated IL leaching was supported by an increase in BET surface areas and porosity measurements (Table 4) for the used SCILLs. All catalysts showed characteristic Type IV isotherms with H3 hysteresis loops (Figure S3). The result of IL leaching was further shown by changes in the pore shapes (shown by the adsorption/desorption isotherms, Figure S3a) of the fresh and used SCILLs, where the narrowest isotherm was found for the used 2 ML coated catalyst, suggesting that a greater degree of leaching occurred over this catalyst, which was supported by TGA measurements.

Table 4. Surface area and particle size measurements of all Pd-based catalysts.

IL/Organic Modifier	Surface Area (m^2/g)	Pore Volume (cm^3/g)	Pore Diameter (nm)
1Pd9Ag/Al_2O_3 (fresh)	209 ± 0.8	0.58	7.9
1Pd9Ag/Al_2O_3 (used)	187 ± 0.5	0.48	7.2
1Pd9Ag-14%$[N_{4444}][NO_3]$ (fresh)	172 ± 1.3	0.43	6.5
1Pd9Ag-14%$[N_{4444}][NO_3]$ (used)	194 ± 1.6	0.45	7.2
1Pd9Ag-24%$[N_{4444}][NO_3]$ (fresh)	103 ± 1.4	0.23	6.7
1Pd9Ag-24%$[N_{4444}][NO_3]$ (used)	147 ± 0.5	0.37	7.0

Figure S3b shows pore size distribution plots for each fresh and used SCILL. The bare and SCILL systems showed wide pore size distributions in the range of 20–150 nm. The pore size distribution measurements of the used SCILL at 2 ML coverage confirmed pore emptying and thus leaching of the IL. Hence, a wider pore size distribution curve was observed compared to the fresh SCILL with 2 ML coverage.

Figure S3c,d show the cumulative pore area and pore volume plots *vs* the average pore diameter to show the effect on the porosity as the weight loading of the ionic liquid is increased. An increase in pore volume and area in the SCILLs post-reaction was seen in these plots, further implying that as the loading of the IL increased, so did the degree of leaching, causing partial emptying of the pores and, thus, approaching the pore volume and size of the fresh uncoated catalysts.

STEM line scan measurements and HR-TEM particle size analyses were performed on selected fresh (Figures S4–S6, Supplementary Materials) and used SCILL systems that were active in the selective hydrogenation of 1,7-octadiene to 1-octene. BSE images (Figure 7a,c,e) of the used catalysts showed areas of bright spots indicative of Pd and Ag. Line scans (EDX spectra provided in the Supplementary Materials, Figure S7) in Figure 7d,f confirm the presence of the ionic liquids post-reaction. This confirms that despite some IL leaching (as seen by thermal analyses), there remained ionic liquid on the surface of the catalyst—in sufficient quantity to exhibit ligand properties, which improved the selectivity to 1-octene up to 2 ML IL coverage. Interestingly, the loss of ionic liquid can be further seen by a spatial distribution of nitrogen, presenting a low signal for both used SCILLs (Figure 7d,f).

TEM images showed the formation of some large agglomerates (Figure 8a–c) in the used catalysts compared to their fresh counterparts (Figure S8, Supplementary Materials). Particle size measurements of approximately 100 particles gave average diameters of 8.9 nm, 9.3 nm, and 7.5 nm for the used 1Pd9Ag/Al_2O_3, 1Pd9Ag-14%$[N_{4444}][NO_3]$, and 1Pd9Ag-24%$[N_{4444}][NO_3]$ catalysts, respectively, compared to their initial sizes of 5.9 nm, 9.0 nm, and 18.4 nm seen in their fresh counterparts. Smaller particle sizes noted over the 2 ML-coated catalyst suggest that with the loss of almost 14% of the ionic liquid (see TGA section), the metal support interaction became stronger once again as the catalyst having

exposed Ag sites could have been re-reduced during the reaction. XPS measurements (shown later) of the fresh uncoated bimetallic catalyst revealed the presence of PdO species that would reduce upon exposure to hydrogen. Large particle size distributions were also evident for all used catalysts (Figure 8d–f).

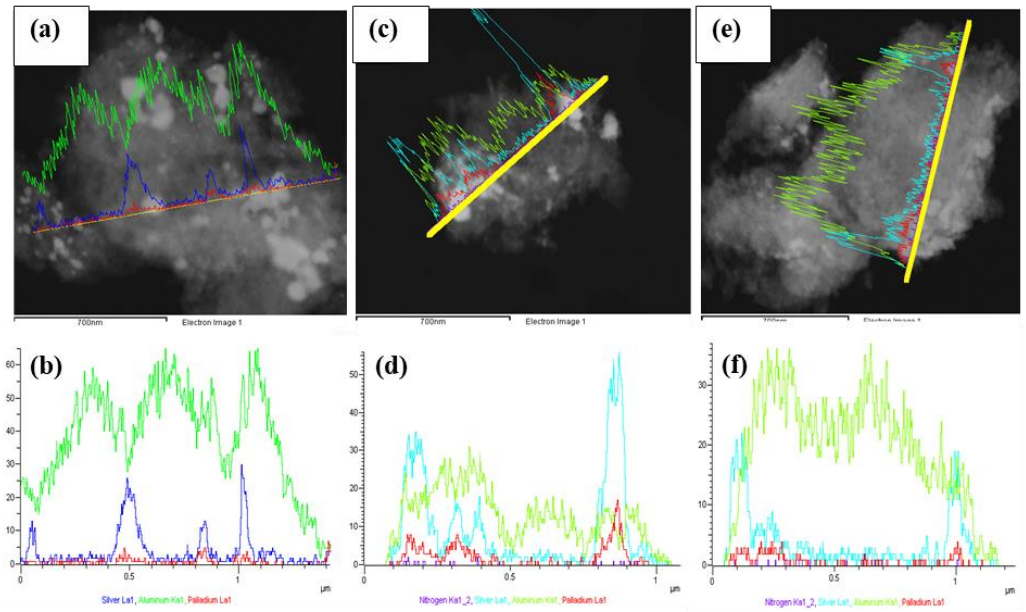


Figure 7. STEM-EDX line scans over the used catalysts showing (**a**) BSE image of 1Pd9Ag/Al_2O_3; (**b**) combined line scans of Pd, Ag, and Al; (**c**) BSE image of 1Pd9Ag-14%[N_{4444}][NO_3], (**d**) combined line scans of Pd, Ag, Al, and N; (**e**) BSE image of 1Pd9Ag-24%[N_{4444}][NO_3]; (**f**) combined line scans of Pd, Ag, Al, and N.

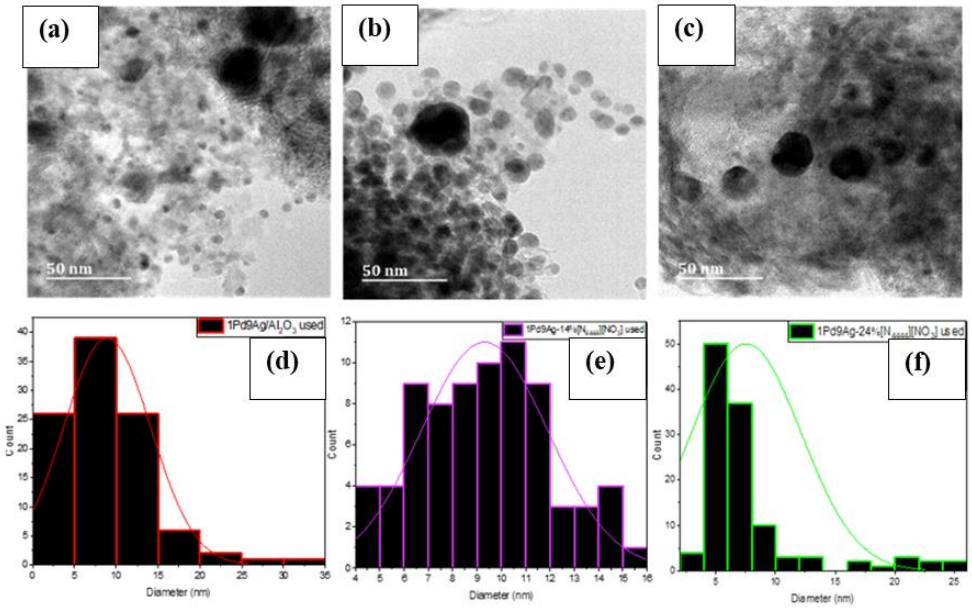


Figure 8. STEM-EDX images of used (**a**) 1Pd9Ag/Al_2O_3, (**b**) 1Pd9Ag-14%[N_{4444}][NO_3], and (**c**) 1Pd9Ag-24%[N_{4444}][NO_3] catalysts with their respective particle size distribution graphs (**d**–**f**).

2.4. XPS

XP spectra for the fresh and used uncoated and coated catalysts are shown in Figure 9. The Pd 3d XP spectra for all catalysts showed two peaks at binding energies of ~335 eV and ~340 eV, which correspond to the spin–orbit split 3d level of Pd and are due to Pd^0 species [50]. Pd^{2+} species (in the form of PdO) are responsible for the higher binding energy peaks observed at ~338 eV and ~343 eV for the $3d_{5/2}$ and $3d_{3/2}$ components, respectively [50]. The large amount of Pd^{2+} species in the SCILLs are due to complexation of Pd with the anion [26]. All used catalysts showed an increase in the PdO species that had sharper peak intensities compared to their fresh counterparts (Figure 9b,d) due to IL rearrangement on the catalyst surface as a result of leaching.

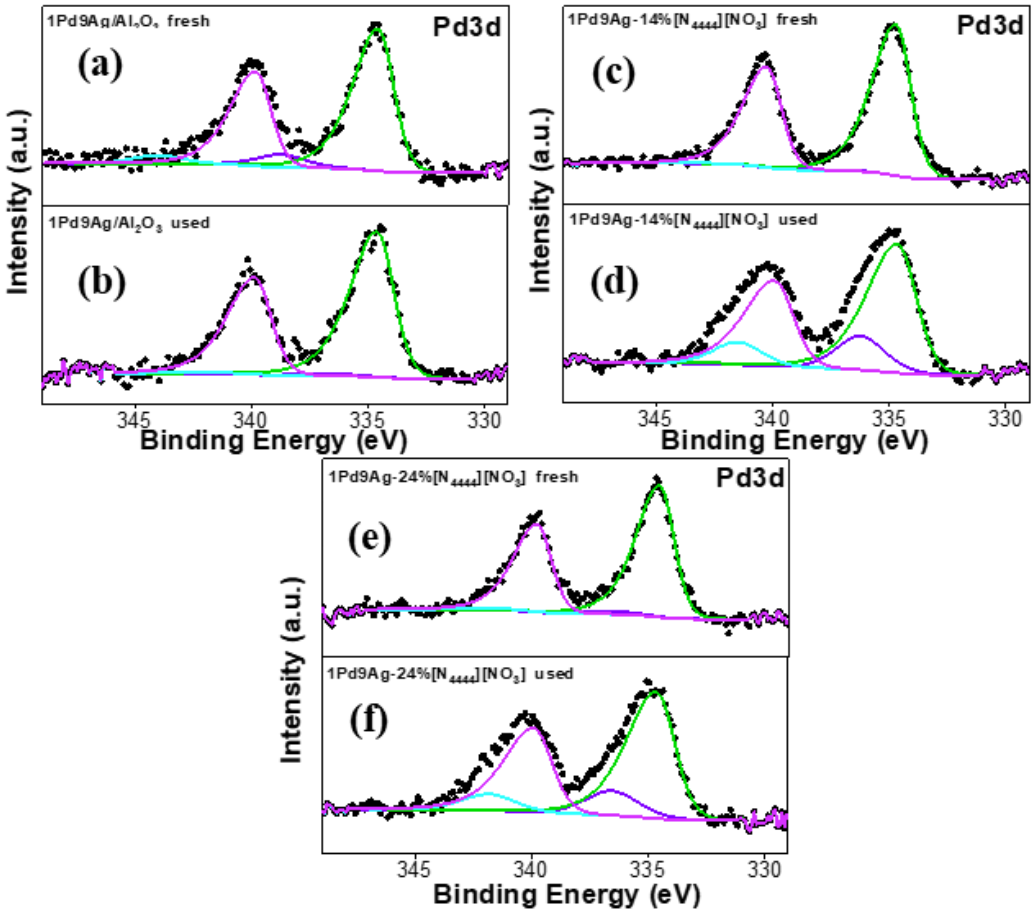


Figure 9. Pd 3d XP spectra for the fresh and used catalysts: fresh $1Pd9Ag/Al_2O_3$ (**a**), used $1Pd9Ag/Al_2O_3$ (**b**), fresh $1Pd9Ag\text{-}14\%[N_{4444}][NO_3]$ (**c**), used $1Pd9Ag\text{-}14\%[N_{4444}][NO_3]$ (**d**), fresh $1Pd9Ag\text{-}24\%[N_{4444}][NO_3]$ (**e**) and used $1Pd9Ag\text{-}24\%[N_{4444}][NO_3]$ (**f**). Solid black curves represent the raw data. Fitted individual components are also shown by solid-coloured curves.

The two prominent peaks (~367 eV and ~373 eV) in the Ag 3d XP spectra (Figure 10) for the $3d_{5/2}$ and $3d_{3/2}$ spin orbitals, respectively, demonstrate the presence of Ag^0 [51]. The higher binding energy peaks at ~370 eV and ~376 eV in all catalysts are assigned to satellite peaks [52]. No peaks suggesting the presence of silver oxide species (367–368 eV) were found [52].

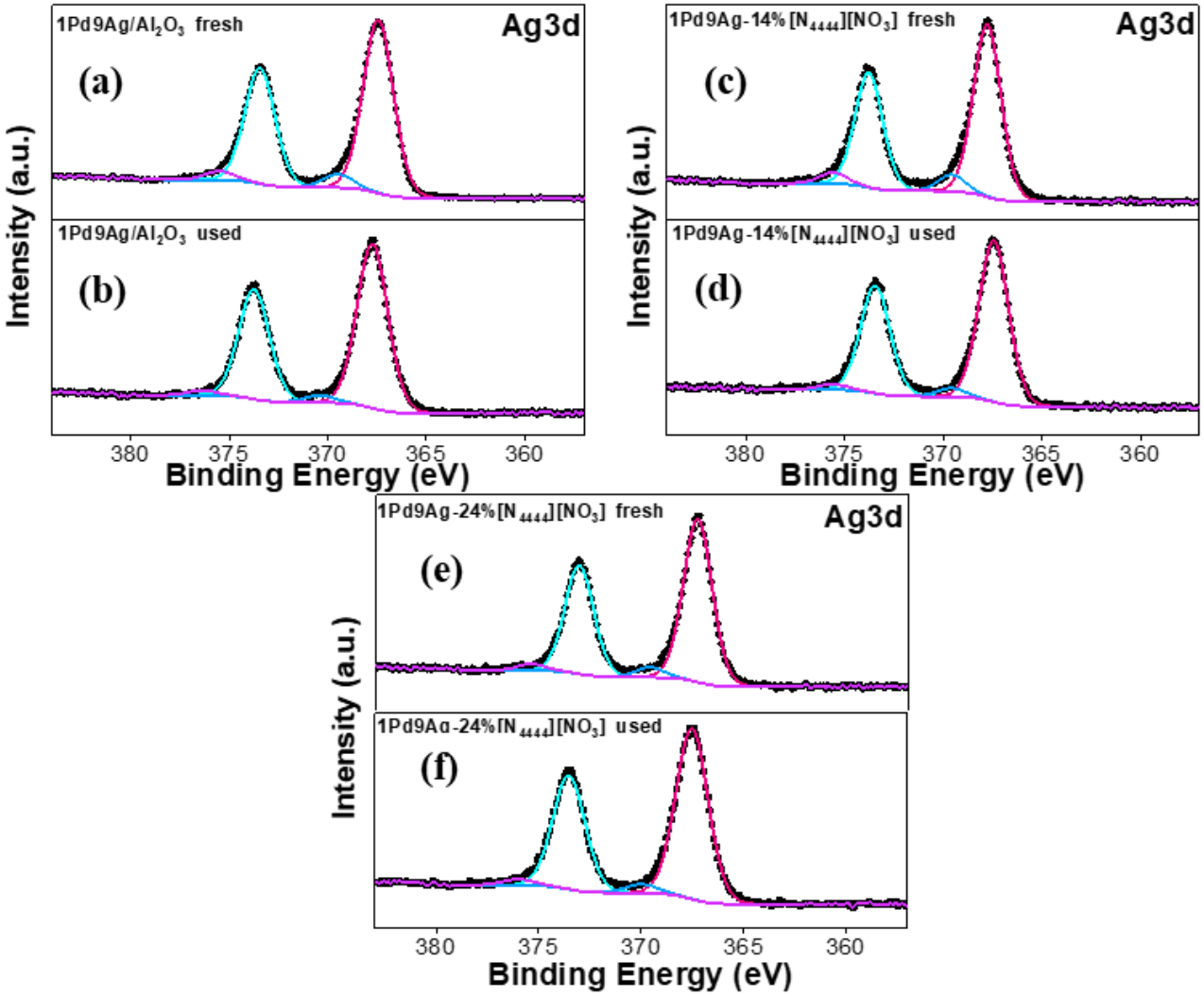


Figure 10. Ag 3d XP spectra for the fresh and used catalysts: fresh 1Pd9Ag/Al_2O_3 (**a**), used 1Pd9Ag/Al_2O_3 (**b**), fresh 1Pd9Ag-14%[N_{4444}][NO_3] (**c**), used 1Pd9Ag-14%[N_{4444}][NO_3] (**d**), fresh 1Pd9Ag-24%[N_{4444}][NO_3] (**e**) and used 1Pd9Ag-24%[N_{4444}][NO_3] (**f**).Solid black curves represent the raw data. Fitted individual components are also shown by solid-coloured curves.

The N 1s XP spectra for the fresh and used SCILLs are shown in Figure 11. The single broad N 1s peak was fitted by two components assigned to nitrogen atoms of nitride -N= (398–399 eV) and -N-(C=O) at ~400–401 eV [53]. The presence of the carbonyl species suggests a possible partial decomposition of the nitrate anion (not detected in the fresh and used SCILLs) initiated by the presence of acetone that may not have been completely removed during the coating process (SCILL synthesis). In the used coated catalysts (Figure 11b,d), the intensities of the nitride and organic nitrogen components were now significantly lower than those of their fresh SCILLs, indicating a high degree of IL decomposition. This substantiates the surface area and TEM analyses, where increased surface areas and smaller particle sizes in the used SCILLs, respectively, were evident. The observed signal-to-noise ratio was low, further implying a low content of nitrogen in the samples.

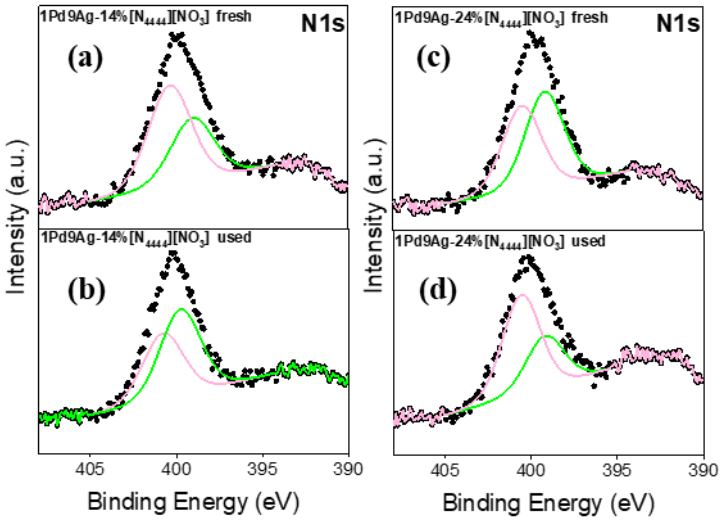


Figure 11. N 1s XP spectra for the fresh and used catalysts: fresh 1Pd9Ag-14%[N_{4444}][NO_3] (**a**), used 1Pd9Ag-14%[N_{4444}][NO_3] (**b**), fresh 1Pd9Ag-24%[N_{4444}][NO_3] (**c**) and used 1Pd9Ag-24%[N_{4444}][NO_3] (**d**). Solid black curves represent the raw data. Fitted individual components are also shown by solid-coloured curves.

Figure 12 shows the C 1s XP spectra for the fresh and used SCILL samples. Three features were seen, aliphatic chain carbon (C_4H_9) at ~285 eV, ammonium coupled carbon (-CH_2-N) at ~286 eV, and the C=O component at ~288 eV [54]. The carbonyl species detected at higher binding energy (present in both fresh and used SCILLs) confirms that the acetone solvent (in the unused catalysts) may have reacted with the IL/substrate to give C=O products.

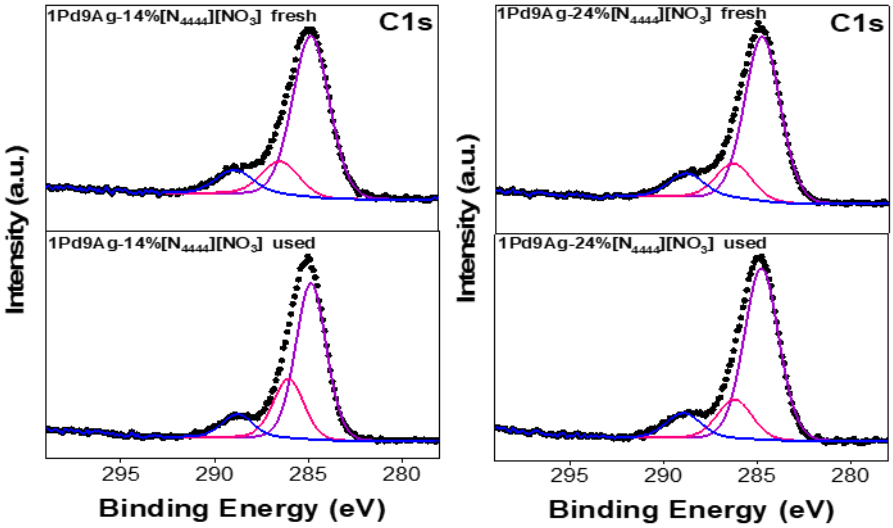


Figure 12. C 1s XP spectra for the fresh and used [N_{4444}][NO_3]-coated catalysts. Solid black curves represent the raw data. Fitted individual components are also shown by solid-coloured curves.

Additional Al 2p, O1s, and survey XP spectra are presented in the Supplementary Materials. In Figure S9 (Supplementary Materials), the main Al 2p signal at ~74 eV in all catalysts is due to the Al-O bond present in alumina [55]. The smaller component at higher binding energy is also attributed to alumina and is due to spin–orbit coupling that splits the energy level in two. The O 1s XP spectra in Figure S10 (Supplementary Materials) represent two features with the main component at ~531 eV due to alumina and the second component at ~532 eV due to adsorbed moisture [56]. The intensity of the higher binding

energy peak increased in the used SCILLs due to the loss of IL during the reaction, which allowed a higher accumulation of moisture.

3. Experiment

3.1. Catalyst Preparation

The 1Pd9Ag/Al_2O_3 catalyst was prepared by deposition precipitation using palladium nitrate dihydrate (Sigma-Aldrich, Johannesburg, South Africa, 99.9%) and silver nitrate hexahydrate (Sigma-Aldrich, Johannesburg, South Africa, 99.9%) as metal precursors, and gamma alumina (Merck, Johannesburg, South Africa, 99%) as the support material. The pH of the support solution was adjusted to 10 using 25% ammonia solution. All uncoated catalysts were dried under vacuum at 70 °C over 6–8 h using a rotary evaporator prior to oven-drying overnight at 110 °C. The catalysts were calcined at 500 °C for 8 h and activated under hydrogen atmosphere (100%) at 300 °C for 4 h using a flow rate of 40 mL/min. Modification of the 1Pd9Ag/Al_2O_3 catalyst with [N_{4444}][NO_3] (Sigma-Aldrich, Johannesburg, South Africa, 97%) was carried out by introducing the ionic-liquid–acetone mixture to a round bottom flask containing a solution of the solid catalyst suspended in acetone. The solvent was removed at 60 °C under vacuum using a rotary evaporator until a dry powder was obtained. The SCILLs were further dried under vacuum for 3 h prior to catalytic testing with coding: 1Pd9Ag-14%[N_{4444}][NO_3], 1Pd9Ag-24%[N_{4444}][NO_3], and 1Pd9Ag-33%[N_{4444}][NO_3].

3.2. Brunauer–Emmett–Teller (BET) Measurements

Surface area, pore volume, and pore size distribution analyses were performed on a Micromeritics TriStar II 3020 instrument. The temperature was maintained at −195 °C. Approximately 100 mg of catalyst was degassed at 90 °C for 1 h under nitrogen to remove physisorbed moisture and then at 200 °C for 12 h. For the SCILLs, degassing was performed using the same temperature profile as the uncoated catalysts on a Micromeritics vacprep degasser. All measurements were conducted in triplicate to ensure reproducibility with the reported standard deviations.

3.3. High-Resolution-Transmission Electron Microscopy (HR-TEM)

A spatula tip of the sample (uncoated) was loaded into an Eppendorf vial and sonicated in acetone for approximately 30 min. All samples (including the dry dispersed SCILLs) were coated onto holey carbon grids and placed in a Jeol 1010 TEM instrument (Tokyo, Japan). The catalysts were analysed using the Megaview III software (Olympus, Tokyo, Japan) imaging system at an operating voltage of 100 kV.

3.4. H_2-Chemisorption

Chemisorption experiments using H_2 as the probe molecule were carried out using a Micromeritics ASAP 2020 instrument (Atlanta, GA, USA) in order to determine the metal dispersion, crystallite size, and metal surface area on the bare and coated catalysts. Prior to all analyses, approximately 400 mg of sample was degassed (using a vacprep) under a flow of N_2 at 90 °C for 1 h after which the temperature was increased to 200 °C and held for 12 h. The sample was sandwiched between two layers of quartz wool in a quartz U-tube and reduced under H_2 at 300 °C for 4 h. The analysis was conducted at 100 °C with hydrogen at a 1:0.5 metal-H_2 stoichiometry. Points at 3, 6, 9, 12, 15, 18, 21, 100, 150, 200, 250, 300, 350, and 400 mmHg were taken on the pressure table. The hydrogen uptake capacity was determined by extrapolation to zero pressure.

3.5. Thermal Gravimetric Analysis-Differential Scanning Calorimetry (TGA-DSC)

TGA-DSC analyses were carried out in a PE SDTQ600 instrument (PerkinElmer, Waltham, MA, USA). A small amount of sample was weighed and placed in a sample holder, and the analysis was carried out by heating, under a stream of air, from room temperature to 900 °C at a heating rate of 10 °C/min.

3.6. X-ray Photoelectron Spectroscopy (XPS)

Specimens for X-ray Photoelectron Spectroscopy (XPS) analyses were prepared by pressing a few milligrams of the sample powders onto high-purity indium pellets (Sigma-Aldrich, Johannesburg, South Africa, purity > 99.9%). The XPS analyses were carried out using a Kratos Axis Ultra^{DLD} spectrometer (Manchester, UK) and data were acquired using a monochromatic Al Ka source, operated at 20 mA and 15 kV. Wide scans were acquired at a pass energy of 160 eV and energy step of 1 eV whilst high-resolution spectra were acquired at a pass energy of 10 eV and energy step of 0.1 eV. In both cases, the take-off angle was set at 0° with respect to the sample normal direction. The analysis area was maintained at 300 × 700 microns. During data acquisition, the Kratos charge neutralisation system was used. The neutralisation settings were chosen to have a similar full-width at half-maximum (FWHM) of the Al 2p peak on all the investigated samples.

3.7. Competitive Hydrogenation of a Diene/Octene Mixture

All catalytic studies were carried out in the liquid phase using a continuous, plug flow fixed-bed reactor. For each reaction, a total catalyst bed volume of 4 mL was used where 2 mL of catalyst pellets were diluted in a 1:1 ratio with carborundum. All catalysts were dried under a flow of N_2 (20 mL/min) at 90 °C for 1 h. The hydrogen gas was continuously fed at a set gas hourly space velocity (GHSV) using a Brooks gas flow control box whilst the liquid feed was set at a specific liquid hourly space velocity (LHSV) using a LabAlliance series II isocratic pump. The competitive feed contained 2 wt% 1,7-octadiene and 10 wt% octene in hexane. Each SCILL was optimised for maximum 1-octene selectivity and 1,7-octadiene conversion by varying the reaction temperature and pressure. Reaction products were identified and quantified by a PerkinElmer Clarus 580 Auto System Gas chromatograph (PerkinElmer, Waltham, MA, USA using TotalChrom software (PerkinElmer, Waltham, MA, USA. The column temperature programme involved heating at 40 °C for 15 min followed by a 5 °C/min temperature ramp to 120 °C for 3 min, then at 5 °C/min to 200 °C for 2 min and finally at 20 °C/min to 260 °C for 3 min. All results were obtained in at least duplicate with mass balances between 94 and 101% and carbon balances between 98 and 102%. Equations (1)–(5) were used in the calculations for the catalytic testing in this study.

$$\text{Conversion} = \frac{(\text{mol of diene in} - \text{mol of diene out})}{(\text{mol of diene in})} \times 100 \quad (1)$$

$$\text{Total selectivity}_{(\text{competitive/non}-\text{competitive})} = \frac{(\text{mol 1} - \text{octene detected} + \text{mol internal octenes} + \text{mol octane})}{(\text{total mol of products formed})} \times 100 \quad (2)$$

$$\text{Octene gain} = \frac{(\text{mass octene out} - \text{mass octene in})}{(\text{mass octene in})} \times 100 \quad (3)$$

$$\text{TOF}\left(\text{s}^{-1}\right) = \frac{(\text{mol of substrate converted})}{(\text{mass of catalyst}) \times (\text{time})} \quad (4)$$

$$\text{STY}\left(\frac{\text{g}}{\text{kg.h}}\right) = \frac{(\text{mass of product formed})}{(\text{mol of metal}) \times (\text{time})} \quad (5)$$

4. Summary and Conclusions

A comparison between the organic modifier ([EIM]) and [N_{4444}][NO_3]-coated catalysts showed that the presence of the anion in the SCILL system was necessary to change the product selectively, which was mainly towards octane over the bare and EIM-coated catalysts. Diene conversions of close to 100% were observed over the 1Pd9Ag/Al_2O_3, 1Pd9Ag-14%[N_{4444}][NO_3], 1Pd9Ag-10%[EIM], and 1Pd9Ag-20%[EIM] catalysts with high octane selectivities and zero net gain of 1-octene in the product stream. The conversion of 1,7-octadiene steadily decreased as the surface coverage of the IL and organic modifier

was increased up to 3 ML. Hydrogen chemisorption studies revealed a decline in metal dispersion and H_2 uptakes as the IL surface coverage was increased. The activity of the SCILL was maintained until 2 ML with the highest selectivity of 1-octene (75%) observed over 1Pd9Ag-24%[N_{4444}][NO_3]. A marked decline in 1-octene conversion was observed from the bare catalyst (100%) to 1 ML and 2 ML IL surface coverage. Ionic liquid leaching was confirmed through TGA-DSC, BET, and HR-TEM techniques, revealing a loss of up to 14% of the IL. Particle sizes of the used catalyst coated with 2 ML IL were smaller than those of its fresh counterpart, likely due to IL island formation on the catalyst surface from partial removal of the IL, which exposed bare silver sites that could have been re-reduced during the reaction. BSE line scans still showed the presence of the IL post-reaction, confirming that leaching was only partial. Non-competitive catalytic reactions showed that in the absence of 1-octene, 1,7-octadiene conversion reached 100% across the bare, organically modified, and SCILL systems at 1 ML coverage. A decreasing octane selectivity trend was further seen for these catalysts (3 ML > 2 ML > 1 ML). The IL coating did reduce the octene isomerisation reaction and both solvent and ligand effects were responsible for the different product selectivities. For the non-competitive 1-octene mixture, at 60% isoconversion, the selectivity to octane was still high over the SCILL, implying the need for a competing substrate to hinder sites selective for the total hydrogenation reaction.

Supplementary Materials: The following supporting information can be downloaded at: https://www.mdpi.com/article/10.3390/catal13040746/s1, Figure S1: Solubility tests of (a) [N_{4444}][NO_3] and (b) [EMIM] in 1,7-octadiene, 1-octene and hexane; Figure S2: Weight loss and derivative weight % curves of the fresh and used 1Pd9Ag/Al_2O_3 catalysts coated with [N_{4444}][NO_3] corresponding to 1 ML, 2ML and 3 ML; Figure S3: BET measurements of the fresh and used PdAg/Al_2O_3-SCILL systems showing (a) N_2 adsorption/desorption isotherms, (b) pore size distribution plots, (c) cumulative pore area and (d) cumulative pore volume; Figure S4: STEM-EDX line scans over the fresh 1Pd9Ag/Al_2O_3 catalyst showing (a) BSE image, (b) line scan of Pd (red), (c) line scan of Ag (blue), (d) line scan of Al (green) and (e) combined line scans of Pd, Ag and Al; Figure S5: STEM-EDX line scans over the fresh 1Pd9Ag-14%[N_{4444}][NO_3] catalyst showing (a) BSE image, (b) line scan of Pd (red), (c) line scan of Ag (cyan), (d) line scan of Al (green), (e) line scan of N (blue) and (e) combined line scans of Pd, Ag and Al and N; Figure S6: STEM-EDX line scans over the fresh 1Pd9Ag-24%[N_{4444}][NO_3] catalyst showing (a) BSE image, (b) line scan of Pd (red), (c) line scan of Ag (cyan), (d) line scan of Al (green), (e) line scan of N (blue) and (e) combined line scans of Pd, Ag and Al and N; Figure S7: EDX spectra of the used catalysts: (a) 1Pd9Ag/Al_2O_3, (b) 1Pd9Ag-14%[N_{4444}][NO_3] and (c) 1Pd9Ag-24%[N_{4444}][NO_3]; Figure S8: STEM-EDX images of fresh (a) 1Pd9Ag/Al_2O_3, (b) 1Pd9Ag-14%[N_{4444}][NO_3] and (c) 1Pd9Ag-24%[N_{4444}][NO_3] catalysts with their respective particle size distribution graphs (d-f); Figure S9: Al 2p XP spectra for the fresh and used uncoated and [N_{4444}][NO_3] coated catalysts. Solid black curves represent the raw data. Fitted individual components are also shown, by solid coloured curves; Figure S10: O 1s XP spectra for the fresh and used uncoated and [N_{4444}][NO_3] coated catalysts. Solid black curves represent the raw data. Fitted individual components are also shown, by solid coloured curves; Figure S11: XPS survey spectra for the fresh and used uncoated and [N_{4444}][NO_3] coated catalysts.

Author Contributions: Conceptualization, R.C. and H.B.F.; methodology, R.C.; software, R.C. and M.P.; validation, H.B.F. and M.P.; formal analysis, R.C. and M.P.; investigation, R.C.; resources, H.B.F. and M.P.; data curation, R.C. and M.P.; writing—original draft preparation, R.C.; writing—review and editing, R.C., M.L.S., M.P. and H.B.F.; visualization, R.C., H.B.F. and M.P.; supervision, H.B.F. and M.L.S.; project administration, H.B.F.; funding acquisition, H.B.F. All authors have read and agreed to the published version of the manuscript.

Funding: This research was funded by the NRF (grant 111660).

Data Availability Statement: Data is contained within the article or Supplementary Materials. Data and work referenced in this manuscript can be accessed at: https://doi.org/10.1002/cctc.202201043 (accessed on 30 January 2023) and https://doi.org/10.1016/j.mcat.2022.112344 (accessed on 30 January 2023).

Acknowledgments: We are grateful to the University of KwaZulu-Natal, SASOL, and the NRF (grant 111660) for financial assistance.

Conflicts of Interest: The authors declare that there is no conflict of interest.

References

1. Liu, L.; Tai, X.; Zhou, X.; Liu, L.; Zhang, X.; Ding, L.; Zhang, Y. Au–Pt bimetallic nanoparticle catalysts supported on UiO-67 for selective 1,3-butadiene hydrogenation. *J. Taiwan Inst. Chem. Eng.* **2020**, *114*, 220–227. [CrossRef]
2. Yardimci, D.; Serna, P.; Gates, B.C. Tuning Catalytic Selectivity: Zeolite- and Magnesium Oxide-Supported Molecular Rhodium Catalysts for Hydrogenation of 1,3-Butadiene. *ACS Catal.* **2012**, *2*, 2100–2113. [CrossRef]
3. Bu, W.; Zhao, L.; Zhang, Z.; Zhang, X.; Gao, J.; Xu, C. Effect of water on hydrogenation of 1,3-butadiene over Au (111): A joint theoretical and experimental study. *Appl. Surf. Sci.* **2014**, *289*, 6–13. [CrossRef]
4. Yardimci, D.; Serna, P.; Gates, B.C. A Highly Selective Catalyst for Partial Hydrogenation of 1,3-Butadiene: MgO-Supported Rhodium Clusters Selectively Poisoned with CO. *ChemCatChem* **2012**, *4*, 1547–1550. [CrossRef]
5. Méndez, F.J.; Piccolo, L.; Solano, R.; Aouine, M.; Villasana, Y.; Guerra, J.; Curbelo, S.; Olivera-Fuentes, C.; Brito, J.L. Promoting effect of ceria on the performance of NiPd/CeO_2–Al_2O_3 catalysts for the selective hydrogenation of 1,3-butadiene in the presence of 1-butene. *New J. Chem.* **2018**, *42*, 11165–11173. [CrossRef]
6. Jalal, A.; Uzun, A. An ordinary nickel catalyst becomes completely selective for partial hydrogenation of 1,3-butadiene when coated with tributyl(methyl)phosphonium methyl sulfate. *Appl. Catal. A Gen.* **2018**, *562*, 321–326. [CrossRef]
7. Gunasekar, G.H.; Jung, K.D.; Yoon, S. Hydrogenation of CO_2 to Formate using a Simple, Recyclable, and Efficient Heterogeneous Catalyst. *Inorg. Chem.* **2019**, *58*, 3717–3723. [CrossRef] [PubMed]
8. Liu, L.; Tai, X.; Zhou, X. Au^{3+}/Au^0 Supported on Chromium(III) Terephthalate Metal Organic Framework (MIL-101) as an Efficient Heterogeneous Catalystfor Three-Component Coupling Synthesis of Propargylamines. *Materials* **2017**, *10*, 99. [CrossRef]
9. Krier, J.M.; Michalak, W.D.; Cai, X.; Carl, L.; Komvopoulos, K.; Somorjai, G.A. Sum Frequency Generation Vibrational Spectroscopy of 1,3-Butadiene Hydrogenation on 4 nm Pt@SiO_2, Pd@SiO_2, and Rh@SiO_2 Core–Shell Catalysts. *Nano Lett.* **2015**, *15*, 39–44. [CrossRef]
10. Liu, C.; Yang, K.; Zhao, J.; Pan, Y.; Liu, D. Hydrogenation of 1,3-butadiene over Au and Pt/SiO_2-N catalysts at low temperature. *Catal. Commun.* **2015**, *67*, 72–77. [CrossRef]
11. Guo, Y.; Yang, J.; Zhuang, J.; Sun, H.; Zhang, H.; Yue, Y.; Zhu, H.; Bao, X.; Yuan, P. Selectively catalytic hydrogenation of styrene-butadiene rubber over Pd/g-C_3N_4 catalyst. *Appl. Catal. A Gen.* **2020**, *589*, 117312. [CrossRef]
12. Jalal, A.; Uzun, A. An exceptional selectivity for partial hydrogenation on a supported nickel catalyst coated with [BMIM][BF_4]. *J. Catal.* **2017**, *350*, 86–96. [CrossRef]
13. Katano, S.; Kato, H.S.; Kawai, M.; Domen, K. Partial Hydrogenation of 1,3-Butadiene on Hydrogen-Precovered Pd(110) in the Balance of π-Bonded C4 Hydrocarbon Reactions. *J. Phys. Chem. C.* **2008**, *112*, 17219–17224. [CrossRef]
14. Zhang, X.; Shi, H.; Xu, B.Q. Catalysis by Gold: Isolated Surface Au^{3+} Ions are Active Sites for Selective Hydrogenation of 1,3-Butadiene over Au/ZrO_2 Catalysts. *Angew. Chem. Int. Ed.* **2005**, *44*, 7132–7135. [CrossRef] [PubMed]
15. Valcárcel, A.; Clotet, A.; Ricart, J.M.; Delbecq, F.; Sautet, P. Comparative DFT study of the adsorption of 1,3-butadiene, 1-butene and 2-cis/trans-butenes on the Pt(111) and Pd(111) surfaces. *Surf. Sci.* **2004**, *549*, 121–133. [CrossRef]
16. Yan, H.; Cheng, H.; Yi, H.; Lin, Y.; Yao, T.; Wang, C.; Li, J.; Wei, S.; Lu, J. Single-Atom Pd1/Graphene Catalyst Achieved by Atomic Layer Deposition: Remarkable Performance in Selective Hydrogenation of 1,3-Butadiene. *JACS* **2015**, *137*, 10484–10487. [CrossRef]
17. Hugon, A.; Delannoy, L.; Krafft, J.-M.; Louis, C. Selective Hydrogenation of 1,3-Butadiene in the Presence of an Excess of Alkenes over Supported Bimetallic Gold−Palladium Catalysts. *J. Phys. Chem. C* **2010**, *114*, 10823–10835. [CrossRef]
18. Yang, D.; Odoh, S.O.; Borycz, J.; Wang, T.C.; Farha, O.K.; Hupp, J.T.; Cramer, C.J.; Gagliardi, L.; Gates, B.C. Tuning Zr_6 Metal–Organic Framework (MOF) Nodes as Catalyst Supports: Site Densities and Electron-Donor Properties Influence Molecular Iridium Complexes as Ethylene Conversion Catalysts. *ACS Catal.* **2016**, *6*, 235–247. [CrossRef]
19. Chen, G.; Xu, C.; Huang, X.; Ye, J.; Gu, L.; Li, G.; Tang, Z.; Wu, B.; Yang, H.; Zhao, Z.; et al. Interfacial electronic effects control the reaction selectivity of platinum catalysts. *Nat. Mater.* **2016**, *15*, 564–569. [CrossRef]
20. Welton, T. Ionic liquids in catalysis. *Coord. Chem. Rev.* **2004**, *248*, 2459–2477. [CrossRef]
21. Steinrück, H.P.; Libuda, J.; Wasserscheid, P.; Cremer, T.; Kolbeck, C.; Laurin, M.; Maier, F.; Sobota, M.; Schulz, P.S.; Stark, M. Surface Science and Model Catalysis with Ionic Liquid-Modified Materials. *Adv. Mater.* **2011**, *23*, 2571–2587. [CrossRef] [PubMed]
22. Babucci, M.; Uzun, A. Effects of interionic interactions in 1,3-dialkylimidazolium ionic liquids on the electronic structure of metal sites in solid catalysts with ionic liquid layer (SCILL). *J. Mol. Liq.* **2016**, *216*, 293–297. [CrossRef]
23. Kernchen, U.; Etzold, B.; Korth, W.; Jess, A. Solid Catalyst with Ionic Liquid Layer (SCILL)—A New Concept to Improve Selectivity Illustrated by Hydrogenation of Cyclooctadiene. *Chem. Eng. Technol.* **2007**, *30*, 985–994. [CrossRef]
24. Umpierre, A.P.; Machado, G.; Fecher, G.H.; Morais, J.; Dupont, J. Selective Hydrogenation of 1,3-Butadiene to 1-Butene by Pd(0) Nanoparticles Embedded in Imidazolium Ionic Liquids. *Adv. Synth. Catal.* **2005**, *347*, 1404–1412. [CrossRef]
25. Antonels, N.C.; Benjamin Williams, M.; Meijboom, R.; Haumann, M. Well-defined dendrimer encapsulated ruthenium SCILL catalysts for partial hydrogenation of toluene in liquid-phase. *J. Mol. Catal. A Chem.* **2016**, *421*, 156–160. [CrossRef]

26. Arras, J.; Paki, E.; Roth, C.; Radnik, J.; Lucas, M.; Claus, P. How a Supported Metal Is Influenced by an Ionic Liquid: In-Depth Characterization of SCILL-Type Palladium Catalysts and Their Hydrogen Adsorption. *J. Phys. Chem. C* **2010**, *114*, 10520–10526. [CrossRef]
27. Bauer, T.; Mehl, S.; Brummel, O.; Pohako-Esko, K.; Wasserscheid, P.; Libuda, J. Ligand Effects at Ionic Liquid-Modified Interfaces: Coadsorption of [C2C1Im][OTf] and CO on Pd(111). *J. Phys. Chem. C* **2016**, *120*, 4453–4465. [CrossRef]
28. Babucci, M.; Hoffman, A.S.; Debefve, L.M.; Kurtoglu, S.F.; Bare, S.R.; Gates, B.C.; Uzun, A. Unraveling the individual influences of supports and ionic liquid coatings on the catalytic properties of supported iridium complexes and iridium clusters. *J. Catal.* **2020**, *387*, 186–195. [CrossRef]
29. Chanerika, R.; Shozi, M.L.; Prato, M.; Friedrich, H.B. The Effect of Coating Pd/Al_2O_3 and $PdAg/Al_2O_3$ Catalysts with [BMIM][DCA] for the Selective Hydrogenation of 1-Octyne in 1-Octene. *ChemCatChem* **2023**, *15*, e202201043. [CrossRef]
30. Williams, D.B.; Stoll, M.E.; Scott, B.L.; Costa, D.A.; Oldham, J.W.J. Coordination chemistry of the bis(trifluoromethylsulfonyl)imide anion: Molecular interactions in room temperature ionic liquids. *Chem. Commun.* **2005**, 1438–1440. [CrossRef]
31. Olivier-Bourbigou, H.; Magna, L.; Morvan, D. Ionic liquids and catalysis: Recent progress from knowledge to applications. *Appl. Catal. A Gen.* **2010**, *373*, 1–56. [CrossRef]
32. Nikolaev, S.A.; Smirnov, V.V. Synergistic and size effects in selective hydrogenation of alkynes on gold nanocomposites. *Catal. Today* **2009**, *147*, S336–S341. [CrossRef]
33. Velasco-Vélez, J.J.; Teschner, D.; Girgsdies, F.; Hävecker, M.; Streibel, V.; Willinger, M.G.; Cao, J.; Lamoth, M.; Frei, E.; Wang, R.; et al. The Role of Adsorbed and Subsurface Carbon Species for the Selective Alkyne Hydrogenation Over a Pd-Black Catalyst: An Operando Study of Bulk and Surface. *Top. Catal.* **2018**, *61*, 2052–2061. [CrossRef] [PubMed]
34. Chanerika, R.; Shozi, M.L.; Prato, M.; Friedrich, H.B. The effect of organic modifiers on Ag/Al_2O_3 catalysts for the sequential hydrogenation of 1-octyne *vs* 1-octene. *Mol. Catal.* **2022**, *525*, 112344. [CrossRef]
35. Miller, S.F.; Friedrich, H.B.; Holzapfel, C.W. The Effects of SCILL Catalyst Modification on the Competitive Hydrogenation of 1-Octyne and 1,7-Octadiene versus 1-Octene. *ChemCatChem* **2012**, *4*, 1337–1344. [CrossRef]
36. Sobota, M.; Happel, M.; Amende, M.; Paape, N.; Wasserscheid, P.; Laurin, M.; Libuda, J. Ligand Effects in SCILL Model Systems: Site-Specific Interactions with Pt and Pd Nanoparticles. *Adv. Mater.* **2011**, *23*, 2617–2621. [CrossRef]
37. Garba, M.D.; Jackson, S.D. Catalytic upgrading of refinery cracked products by trans-hydrogenation: A review. *Appl. Petrochem. Res.* **2017**, *7*, 1–8. [CrossRef]
38. Cremer, T.; Kolbeck, C.; Lovelock, K.R.J.; Paape, N.; Wölfel, R.; Schulz, P.S.; Wasserscheid, P.; Weber, H.; Thar, J.; Kirchner, B.; et al. Towards a Molecular Understanding of Cation–Anion Interactions—Probing the Electronic Structure of Imidazolium Ionic Liquids by NMR Spectroscopy, X-ray Photoelectron Spectroscopy and Theoretical Calculations. *Chem. Eur. J.* **2010**, *16*, 9018–9033. [CrossRef]
39. Zahn, S.; Bruns, G.; Thar, J.; Kirchner, B. What keeps ionic liquids in flow? *Phys. Chem. Chem. Phys.* **2008**, *10*, 6921–6924. [CrossRef]
40. Rietzler, F.; May, B.; Steinrück, H.P.; Maier, F. Switching adsorption and growth behavior of ultrathin [C2C1Im][OTf] films on Au(111) by Pd deposition. *Phys. Chem. Chem. Phys.* **2016**, *18*, 25143–25150. [CrossRef]
41. Kim, W.J.; Kang, J.H.; Ahn, I.Y.; Moon, S.H. Deactivation behavior of a TiO_2-added Pd catalyst in acetylene hydrogenation. *J. Catal.* **2004**, *226*, 226–229. [CrossRef]
42. Kang, J.H.; Shin, E.W.; Kim, W.J.; Park, J.D.; Moon, S.H. Selective Hydrogenation of Acetylene on TiO_2-Added Pd Catalysts. *J. Catal.* **2002**, *208*, 310–320. [CrossRef]
43. Sárkány, A.; Révay, Z. Some features of acetylene and 1,3-butadiene hydrogenation on Ag/SiO_2 and Ag/TiO_2 catalysts. *Appl. Catal. A Gen.* **2003**, *243*, 347–355. [CrossRef]
44. Tomas, J.; Tomas, W. *Introduction to the Principles of Heterogeneous Catalysis*; Academic Press: London, UK, 1967.
45. Ibhadon, A.; Kansal, S. The Reduction of Alkynes Over Pd-Based Catalyst Materials—A Pathway to Chemical Synthesis. *Chem. Eng. Technol.* **2017**, *9*, 1000376.
46. Akçay, A.; Balci, V.; Uzun, A. Structural factors controlling thermal stability of imidazolium ionic liquids with 1-n-butyl-3-methylimidazolium cation on γ-Al_2O_3. *Thermochim. Acta* **2014**, *589*, 131–136. [CrossRef]
47. Akçay, A.; Babucci, M.; Balci, V.; Uzun, A. A model to predict maximum tolerable temperatures of metal-oxide-supported 1-n-butyl-3-methylimidazolium based ionic liquids. *Chem. Eng. Sci.* **2015**, *123*, 588–595. [CrossRef]
48. Babucci, M.; Akçay, A.; Balci, V.; Uzun, A. Thermal Stability Limits of Imidazolium Ionic Liquids Immobilized on Metal-Oxides. *Langmuir* **2015**, *31*, 9163–9176. [CrossRef]
49. Babucci, M.; Balci, V.; Akçay, A.; Uzun, A. Interactions of $[BMIM][BF_4]$ with Metal Oxides and Their Consequences on Stability Limits. *J. Phys. Chem. C* **2016**, *120*, 20089–20102. [CrossRef]
50. Zhao, Z.; Flores Espinosa, M.M.; Zhou, J.; Xue, W.; Duan, X.; Miao, J.; Huang, Y. Synthesis of surface controlled nickel/palladium hydride nanodendrites with high performance in benzyl alcohol oxidation. *Nano Res.* **2019**, *12*, 1467–1472. [CrossRef]
51. Jablonska, M.; Nocun, M.; Bidzińska, E. Silver–Alumina Catalysts for Low-Temperature Methanol Incineration. *Catal. Lett.* **2016**, *146*, 937–944. [CrossRef]
52. Dolatkhah, A.; Jani, P.; Wilson, L. Redox-Responsive Polymer Template as an Advanced Multifunctional Catalyst Support for Silver Nanoparticles. *Langmuir* **2018**, *34*, 341–350. [CrossRef] [PubMed]
53. Dziembaj, R.; Piwowarska, Z. X-ray photoelectron spectroscopy (XPS) as a useful tool to characterize polyaniline doped by 12-tungstosilicic, 12-tungstophosphoric and 12-molybdophosphoric acids. *Synth. Met.* **1994**, *63*, 225–232. [CrossRef]

54. Chen, S.; Artiglia, L.; Orlando, F.; Edebeli, J.; Kong, X.; Yang, H.; Boucly, A.; Corral Arroyo, P.; Prisle, N.; Ammann, M. Impact of Tetrabutylammonium on the Oxidation of Bromide by Ozone. *ACS Earth Space Chem.* **2021**, *5*, 3008–3021. [CrossRef] [PubMed]
55. Moffitt, C.; Chen, B.; Wieliczka, D.; Kruger, M. XPS comparison between nanocrystalline γ-alumina and a new high pressure polymorph. *Solid State Commun.* **2000**, *116*, 631–636. [CrossRef]
56. Sobota, M.; Schmid, M.; Happel, M.; Amende, M.; Maier, F.; Steinrück, H.P.; Paape, N.; Wasserscheid, P.; Laurin, M.; Gottfried, J.M.; et al. Ionic liquid based model catalysis: Interaction of [BMIM][Tf2N] with Pd nanoparticles supported on an ordered alumina film. *Phys. Chem. Chem. Phys.* **2010**, *12*, 10610–10621. [CrossRef]

Disclaimer/Publisher's Note: The statements, opinions and data contained in all publications are solely those of the individual author(s) and contributor(s) and not of MDPI and/or the editor(s). MDPI and/or the editor(s) disclaim responsibility for any injury to people or property resulting from any ideas, methods, instructions or products referred to in the content.